Journal of Seismology **7:** 413–429, 2003.

Non-linear filter, using the wavelet transform, applied to seismological records

A. Pazos[1], M.J. González[2] & G. Alguacil[3,4]
[1]*Real Instituto y Observatorio de la Armada, Cecilio Pujazón s/n, 1100 San Fernando, Cádiz, Spain, e-mail: pazos@roa.es;* [2]*Dpto. de Matemáticas, Universidad de Cádiz, 11510 Pto. Real, Cádiz, Spain, e-mail: majose.gonzalez@uca.es;* [3]*Instituto Andaluz de Geofísica, Observatorio de la Cartuja, Universidad de Granada, 18.071 Granada, Spain, e-mail: alguacil@iag.ugr.es;* [4]*Dpto. de Física Teórica y del Cosmos, Facultad de Ciencias, Universidad de Granada, 18.071 Granada*

Received 24 June 2001; accepted in revised form 16 May 2002

Key words: de-noising, seismic signals, filter, noise, non-linear, signal-noise ratio, wavelet

Abstract

As any process in Nature, seismic records are affected by noise that the analyst would want to eliminate. One of the most common techniques used to minimise this noise effect is the application of linear filters, which reduce the bandwidth of the signal. This method is based on the Fourier Transform, and therefore any perturbation on the coefficients affects the entire record. We have developed a non-linear filter based on the multiresolution analysis of the Discrete Time Wavelet Transform (DTWT). The main idea is to use the time-frequency localisation properties of the wavelet decomposition. Each coefficient is associated to a window on the time-frequency plane, so any perturbation would only affect the time and frequency range of the correspondent window. The procedure we propose has three stages: periodic noise elimination, spikes reduction and, finally, the non-linear filtering. The non-linear filter acts by thresholding the wavelet coefficients. The thresholding estimator will depend on the signal-noise ratio (SNR) in each of the frequency bands associated to the wavelet decomposition. We have compared the proposed method to the coherent structures method (Mallat, 1998) and to two 4^{th} order linear filter banks (Butterworth and Elliptic filters), applying all of them to a synthetic database, and a real earthquake database recorded by the Short Period ROA Network. The proposed method improves the SNR in the 87% of the tested events, being the relative rms error less than three, and the maximum amplitude relative error less than 10% in the 90% of the synthetic database.

Introduction

Any digital or analogue seismic record is always affected by noise due mainly to either natural sources (i.e., wind, water currents, tides) or artificial sources (i.e., traffic, industry), even when the instrument noise is negligible. Besides that, 'spikes', caused by radio transmissions can also be found in the telemetric nets. It is very difficult to build a mathematical model to represent the noise, since it varies from station to station depending on where it is located, or on the time of the day the record is registered.

The short period network of the Royal Naval Observatory (ROA) in San Fernando (Figure 1) is located in the South of Spain. A detection algorithm, based on the well-known STA/LTA algorithm (McEvilly and Majer, 1982), operates over the nine stations of the ROA network. It provides a detection of about 94% of the events identified by the analyst, in spite of the poor signal-noise ratio (SNR) of most of the local events (strong winds from West or East are usually present in this area).

Many phase-picking methods use a filter bank (Evans and Allen, 1983; Gledhill, 1985; Moltshan et al., 1964) or non-sinusoidal transforms (Goforth and Herrin, 1981; Andrew et al., 1882) in order to decompose the signal into several frequency bands and to choose the one with the best SNR.

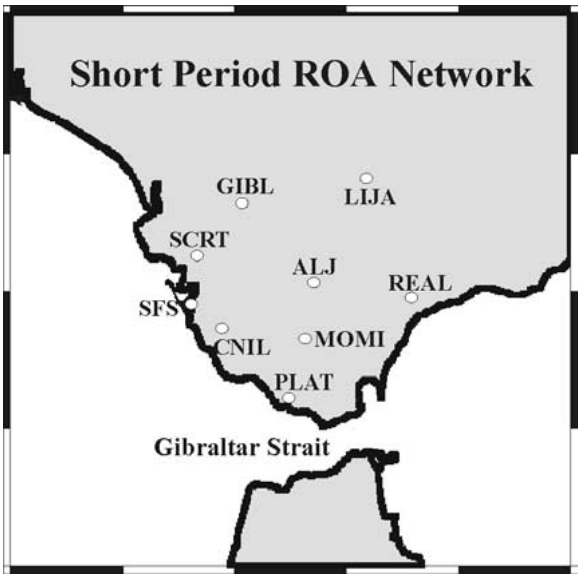

Figure 1. The Short Period ROA Network deployed in the South of Spain composed by nine telemetric seismic stations with 1 Hz. vertical sensors.

When a linear filter is applied, the energy in certain frequency bands is reduced affecting the entire record. These filters are based on the Fourier Transform, which presents a poor resolution on the time-frequency plane: it provides the frequency information content of the signal, but lacks localisation in the time domain. This is because the support of the basis functions covers the entire length of the digital record.

The non-linear filters try to eliminate the noise and to keep the signal information on each of the frequency bands (Donoho, 1994; Ulrych et al., 1999). The idea is to consider local time-frequency transforms, which decompose the signal over waveforms that are well localised in time and frequency. Fedorenko and Husebye (1999) apply non-linear smoothing methods to a polarisation filter output, in their automatic phase picking algorithm for P and S waves.

In this work, we apply a non-linear filtering procedure, using the discrete time wavelet transform (DTWT). We test it on a synthetic and on a real database recorded by the Short Period ROA Network. Noise has been added to the synthetic signal in order to obtain several signal noise ratios.

This method operates directly on the wavelet coefficients and it consists of three steps: periodic noise elimination, spikes reduction and, finally, a non-linear filter as a function of the SNR estimation.

The Discrete Time Wavelet Transform (DTWT) and the multi-resolution analysis

The DTWT is a very useful tool in the analysis of non-stationary signals such as the seismic signals because of its ability to resolve a signal at various scales, that is to perform a multi-resolution analysis. This is mainly a consequence of the specific way the wavelet basis decomposes the time-frequency plane.

An orthonormal wavelet representation of a digital signal, $\boldsymbol{a}_o$, of sample size N, is composed of the set of wavelet coefficients $\{d_j[k]\}$, $1 \le j \le J$ and $0 \le k < N/2^j$, up to a scale $2^J \le N$, plus the remaining low frequency information $\{a_J[k]\}$, $0 \le k < N/2^J$.

A fast discrete algorithm (i.e. Mallat, 1998) that follows a tree diagram based on the iteration of a two FIR filter bank carries out the coefficient calculation. At each stage of the iteration, the input signal is decomposed into high-pass and low-pass components subsampled by 2 as illustrated in Figure 2.

The inverse transform performs the perfect reconstruction of the signal (Figure 2).

The vectors $\tilde{u}$, wavelet filter, and $\tilde{v}$, scaling filter, represent high-pass and low-pass filters respectively that must belong to a perfect reconstruction filter bank. At each stage 'j' of the iteration we obtain detail coefficients 'd_j' that we store, and approximation coefficients 'a_j' that we iterate in order to get the coefficients at the next stage.

The index 'j' is associated with a resolution level that corresponds to the scale 2^j. The approximation coefficients 'a_j' represents the projection of the signal on a level of resolution 'j', and the detail coefficients 'd_{j+1}' represent the increment of the information that is lost when the signal 'a_j' is projected on a coarser level 'j+1'.

Orthonormal wavelets are closely related to these filter bank trees. They provide a simple procedure for designing and building orthonormal basis, composed of dilations and translations of a pair of functions (ψ, ϕ) called wavelet function (or mother wavelet) and scaling function (or father wavelet) respectively (Mallat, 1998).

At each stage 'j' of the filter bank tree, the high-pass signal 'dj' and the low-pass signal 'aj' can be written as:

$$\begin{aligned} d_j[k] &= \langle a_o, \psi_{jk} \rangle \\ 0 \le k &< {}^{N}/_{2^j} \\ a_j[k] &= \langle a_o, \phi_{jk} \rangle \end{aligned} \tag{1}$$

where '<.,.>' denotes the inner product and:

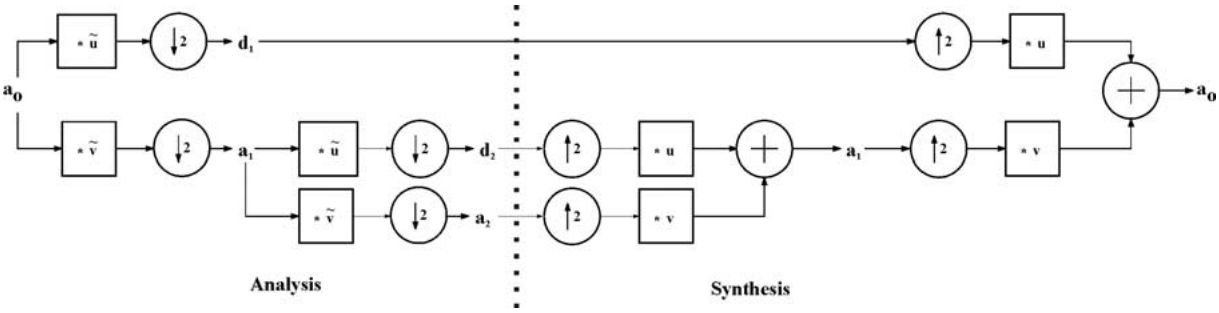

Figure 2. Analysis and Synthesis sections of a two-band filter bank. The filters used determine the perfect reconstruction of the signal. The boxes represent convolution, the circles with downward arrows represent downsampling by a factor of 2 and circles with upward arrows represent upsampling by a factor of 2, which means that a zero is inserted between each sample.

$$\psi_{jk}[n] = \frac{1}{2^{j/2}}\psi\left(\frac{n-2^j k}{2^j}\right)$$

$$\phi_{jk}[n] = \frac{1}{2^{j/2}}\phi\left(\frac{n-2^j k}{2^j}\right)$$

$$n = 0, 1, \ldots, N-1 \qquad (2)$$

At the final stage 'J', the signal 'a_o' gets decompose over the orthonormal basis $\{\{\psi_{jk}\}_{j=1}^{J}, \phi_{Jk}\}$ as:

$$a_o = \sum_{j=1}^{J}\sum_{k=0}^{N/2^j-1} d_j[k]\psi_{jk} + \sum_{k=0}^{N/2^j-1} a_J[k]\phi_{Jk} \qquad (3)$$

The sum $P_J = \sum_k a_J[k]\phi_{Jk}$ can be interpreted as the approximation of a_o at the scale 2^J and $Q_j = \sum_k d_j[k]\psi_{jk}$ as detail variations at scale 2^j, $1 \leq j \leq J$. These detail layers are added up at all scales to progressively improve the approximations of 'a_o', and ultimately recover the original signal a_o.

The multi-resolution analysis, that the orthonormal wavelet bases provide, is mainly a consequence of the specific way they decompose the time-frequency plane. The frequency axis is decomposed in bands whose width has an exponential growth. Each frequency band (Figure 3) is covered by the time-frequency boxes that are uniformly translated in time in order to fill the whole plane. The time-frequency box of each element ψ_{jk} is translated in time by $2^j k$, with a time and frequency width scaled by 2^j and 2^{-j} respectively.

Different tiling of the time-frequency plane can also be considered. A wavelet packet basis divides the frequency axis in separate bands of varying width. They can be designed by using more general filter bank trees (Mallat, 1998). The choice of the tree should depend on the time-frequency localisation properties one would like to obtain.

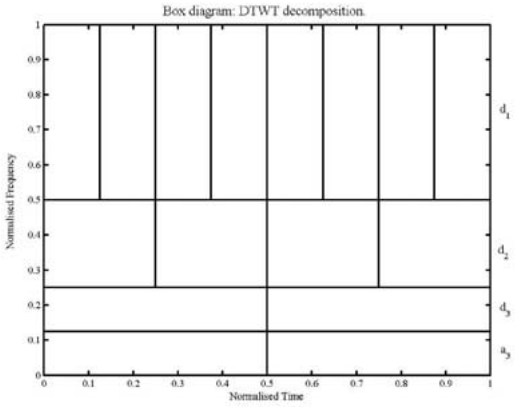

Figure 3. Box diagram: Time-Frequency plane wavelet decomposition to the third level. Time and Frequency axis are normalised and each box corresponds to a wavelet coefficient.

The wavelet used in the DTWT should be chosen depending on the signal. The idea is that the energy or information of the signal should be concentrated on as few coefficients as possible. This depends mostly on the number of vanishing moments of the wavelet and the size of the support (Mallat, 1998). Besides, the wavelet 'library' should try to mach the expected shape of the seismic phase arrivals (Annat and Dowla, 1997). When choosing a particular wavelet, there is a trade-off between the number of vanishing moments and the support size, if the first one increases, so does the second. Daubechies wavelets are optimal in this sense: they have a minimum size for a given number of vanishing moments. After several experiments, we have chosen the Daubechies-8 wavelets since they represent a good compromise between similarity with the seismic waves and localisation on the time domain.

Non-linear techniques

The DTWT has been used extensively in a great number of fields (i.e.: Lilly and Park, 1995; Ridsdill-Smith and Dentith, 1999; Freeden and Schneider, 1998). Applications include denoising of data, smoothing and compression of images.

Mallat (1998) pointed out several techniques of non-linear filtering to remove different kinds of noises. Donoho (1994) proved that in the case of gaussian white noise, nearly optimal estimators are obtained by thresholding decomposition coefficients in an orthonormal wavelet basis.

According to it, the value of the threshold 'T' for estimating a signal in a Gaussian white noise of variance σ^2 should be:

$$T = \sigma\sqrt{2\log_e N} \tag{4}$$

where N is the sample size of the noisy data.

To estimate the variance σ^2 of the noise 'w' from the noisy data '$z = w + f$ ', we need to suppress the influence of the signal 'f'.

The idea is that, for smooth signals 'f', the wavelet coefficients $\langle f, \psi_{1k}\rangle$ are small, and as a result the coefficients $\langle z, \psi_{1k}\rangle \approx \langle w, \psi_{1k}\rangle$ are approximately Gaussian random variables of variance σ^2. In this case, a good estimator for the noise standard deviation is given by the following expression:

$$\sigma = \frac{Median\ (|\langle z, \psi_{1k}\rangle|)_{0\le k<N/2}}{0.6745} \tag{5}$$

Without any a priori knowledge of the type of noise, it is more convenient to use a method that does not involve the noise variance. Mallat (1998, pp. 465–467) proposes, in this case, the coherent structures method: if $\mathcal{B} = \{g_m\}_{0\le m<N}$ is an orthonormal wavelet basis, we progressively extract those vectors of $\mathcal{B}$ that present a better correlation with the noisy data 'z'.

For this we sort out the inner products '$<z,g_m>$':

$$|\langle z, g_{m_k}\rangle| \ge |\langle z, g_{m_{k+1}}\rangle| \quad 0 \le k < N-1 \tag{6}$$

The data z is not reduced to a noise if:

$$\frac{|\langle z, g_{m_o}\rangle|^2}{\|z\|^2} > T_N^2 = \frac{2\log N}{N} \tag{7}$$

For each k≥0, g_{m_k} is a coherent structure if:

$$\frac{|\langle z, g_{m_k}\rangle|^2}{\sum_{p=k}^{N-1} |\langle z, g_{m_p}\rangle|^2} > T_{N-k}^2 \tag{8a}$$

where

$$T_{N-k}^2 = \frac{2\log(N-k)}{N-k} \tag{8b}$$

The algorithm stops when we find the first index k=M such that g_{m_M} is not a coherent structure. Then the signal f is estimated by the sum of the M coherent structures:

$$f = \sum_{k=0}^{M-1} \langle z, g_{m_k}\rangle g_{m_k} \tag{9}$$

Proposed method

We have adapted the coherent structures method (Mallat, 1998) to the seismic records, incorporating some information about the expected seismic signals. Also, we include some considerations about certain noises (we refer to the periodic noises and 'spikes') and instrument responses.

The method has tree steps: periodic noise elimination, spike reduction and non-linear wavelet filter.

Periodic noise elimination

Periodic noises could be characterised by a Fourier series. Therefore, any periodic noise can be considered as a sum of several monochrome noises.

Monochrome noises are detected by analysing the noise spectrum, in the Fourier domain. Those frequencies, f_o, with spectral density values much larger than the mean value computed on a 2 Hz. neighbourhood band (empirically obtained) will be declared monochrome noises.

In order to obtain a better precision than the one allowed by the Fourier Transform ($\Delta f = f_m$/N, where f_m is the sample frequency and N is the sample size of the record), we will carry out the following algorithm:

Let f_o be one of the detected monochrome noise frequencies, and let f_1 and f_2 be two frequencies at distance $\Delta f/2$ of f_o. For each frequency f_i, i = 0,1,2, we approximate the noise data 'w' by:

$$w[n] = A_i \sin(2\pi \tfrac{f_i}{f_m} n + \phi_i) \quad 0 \le n \le N-1 \tag{10}$$

where N is the sample size of the record. The amplitude 'A_i' and the phase 'ϕ_i' are determined for each frequency using the least square method. The frequency that provides the minimum error is chosen to be the new nominal frequency.

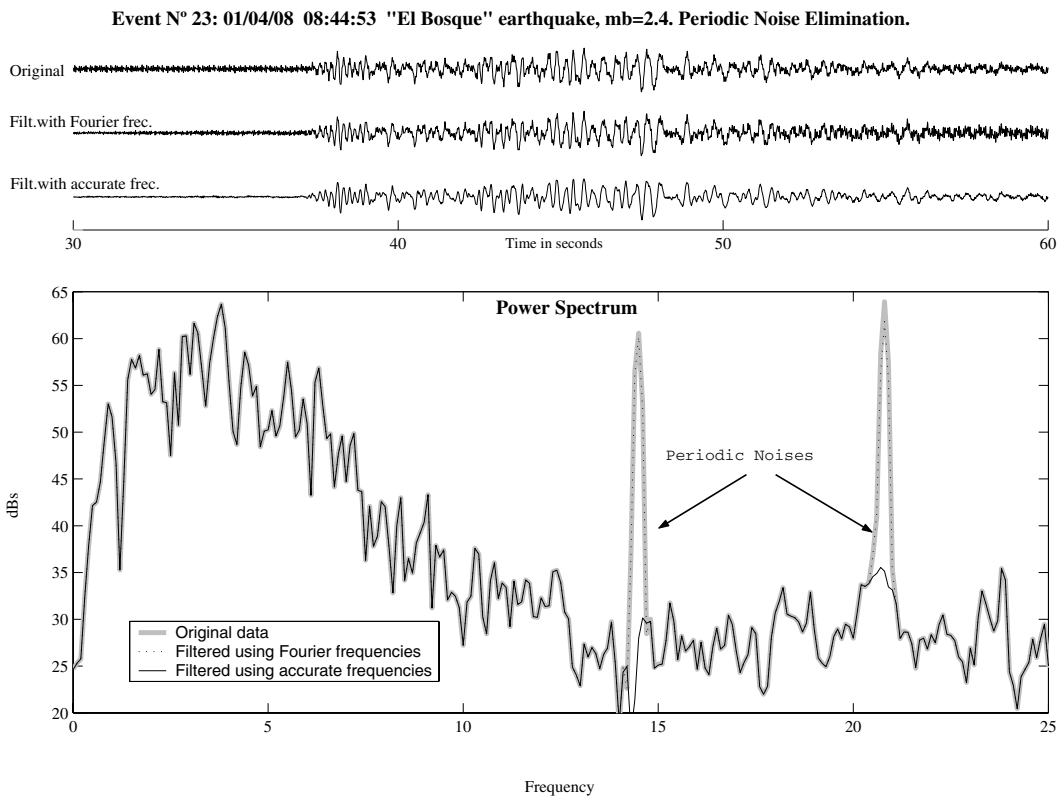

Figure 4. Event number 23 (01/04/08 08:44:53 'El Bosque' earthquake, mb = 2.4) recorded by REAL station: Periodic noise elimination. **Subplot 1:** Original data. **Subplot 2:** Filtered data by periodic noise elimination, using the Fourier frequencies. **Subplot 3:** Filtered data using the accurate frequencies determined by the proposed algorithm. **Subplot 4** shows their power spectrums.

The process is iterated (decreasing the distance to the new nominal frequency by a factor of 2) until we obtain a precision smaller than the 0.01% of the nominal frequency.

In order to avoid possible errors of adjustment due to the spectral content of the entire signal, this procedure is first carried out on the pre-event and later on tested over the entire record.

The Figure 4 shows the real event number 23 (refer to table V: 01/04/08 at 08:44:53 'El Bosque' earthquake mb = 2.4) which contains a periodic noise due to interference, and the result of the periodic noise elimination using the Fourier frequencies and the ones determined by this algorithm.

Spikes reduction

Spikes are commonly due to radio interference and usually one-signed, i.e. either positive or negative. Their short duration and high amplitude characterise them.

The developed algorithm is applied to the wavelet coefficients of the noisy data of sample size N. At each resolution level 'j' in the wavelet decomposition, we estimate the mean and the variance of the energy in a small neighbourhood (left sided and empirically chosen of size 10, 0.1 second) of each of the coefficients '$d_j[k]$', $0 \leq k < N/2^j$. To do so, we consider the following FIR filters:

$$m_k = \sum_{l=k-9}^{k} \frac{d_j^2[l]}{10} \tag{11}$$

$$\sigma_k^2 = \sum_{l=k-9}^{k} \frac{(d_j^2[l] - m_l)^2}{10} \tag{12}$$

In order to avoid impulsive seismic arrivals to be considered spikes, both filters are applied from left to right and right to left. We will say that a coefficient '$d_j[k]$' is produced by a spike if the equation [13] is verified in both directions simultaneously:

$$d_j^2[k] > m_k + 4\sigma_k \tag{13}$$

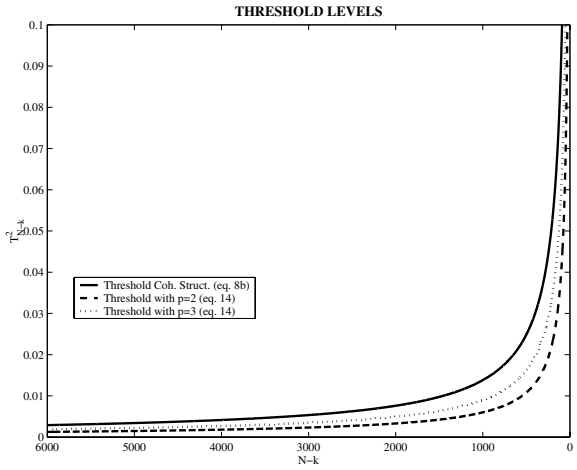

Figure 5. Threshold levels: the solid line represents the threshold values given by the Coherent Structures Method (equation 8-b), and the dotted and dash-dot lines those used in our procedure (Equation 14) for p = 2 and 3 respectively.

In that case, the detected spike is eliminated. Due to the slow decay of the filters, nearby spikes might not be detected. For this reason, the algorithm is applied up to 8 consecutive times or until no more spikes are detected.

The spike detection condition is somehow modified at the windows that correspond to the beginning and end of the record. So, for the first ones we only require equation (13) to be verified backwards (right to left), and only forwards (left to right) for the second ones.

Non-linear wavelet filter

Our method is similar to the coherent structures method described before. The main differences are that the algorithm is applied at each resolution level 'j' of the wavelet decomposition independently, not to the whole record as it is proposed in equation (6), where all the coefficients are considered. So, for each level 'j', we define the thresholds:

$$T^2_{N_j-k} = \frac{p \log_{10}(N_j - k)}{N_j - k} \quad 0 \le k < N_j - 1 \quad (14)$$

where N_j denotes the amount of wavelet coefficients at the level 'j', that is $N/2^j$; and p is a parameter to which we empirically assigned the values 0,2,3 depending on the SNR at that level. Figure 5 shows the threshold values.

In order to estimate the SNR we will assume that the signal 'f' and the noise 'w' are uncorrelated,

$$\|z\|^2 = \|f\|^2 + \|w\|^2 \quad (15)$$

Therefore, the SNR is given by:

$$SNR_{db} = 10 \log_{10}\left(\frac{\|z\|^2}{\|w\|^2} - 1\right) \quad (16)$$

In order to estimate this value at each level 'j', we will assume that the pre-event data provides a good estimation for the entire noise data.

If the **SNR** at level 'j' is **over 40 dB**, the noise is non-significant and we use a value 'p = 0'. Therefore, the corresponding wavelet coefficients are not modified.

When the **SNR is between 10 and 40 dB**, a 'p = 2' value is assigned and all the wavelet coefficients that correspond to non-coherent structures are zeroed. Let us recall that the algorithm is always applied after reordering the wavelet coefficients in a decreasing order of amplitude, i.e. $|d_j[n_k]| \ge |d_j[n_{k+1}]|$

For **SNR between 4 and 10dB**, the value 'p = 3' is applied and therefore the threshold increases. In this case, we also estimate the noise standard deviation, σ_j, using only the coefficients corresponding to the pre-event of the record, according to the equation:

$$\sigma_j = \frac{Median(|d_j[k]|)}{0.6745} \quad (17)$$

where k depends on the pre-event duration.

As before, the wavelet coefficients associated to non-coherent structures are zeroed, but in this case, the ones corresponding to coherent structures are reduced in amplitude by σ_j.

For **SNR between 2.5 and 4 dB**, the procedure described in the previous paragraph is applied, but only in the low frequency levels corresponding to j>3.

In **any other case**, we consider that it is not possible to distinguish the signal from the noise. Hence, all coefficients are zeroed.

Figure 6 shows a scheme of the procedure, applying it to each one of the multi-resolution levels.

Test and database

In order to compare the performance of the different filters, the following parameters could be used:

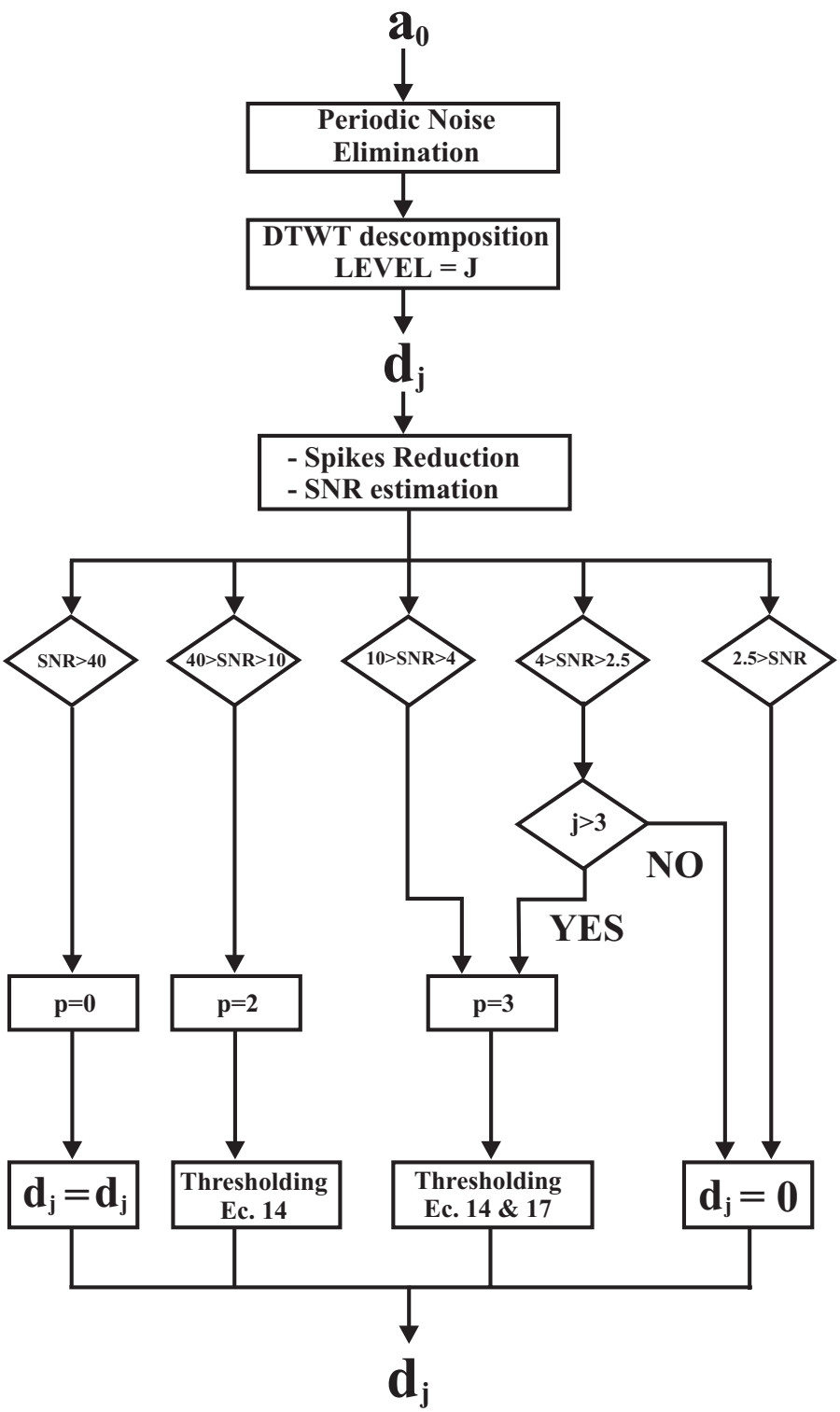

Figure 6. Scheme of the proposed method used for denoising signals.

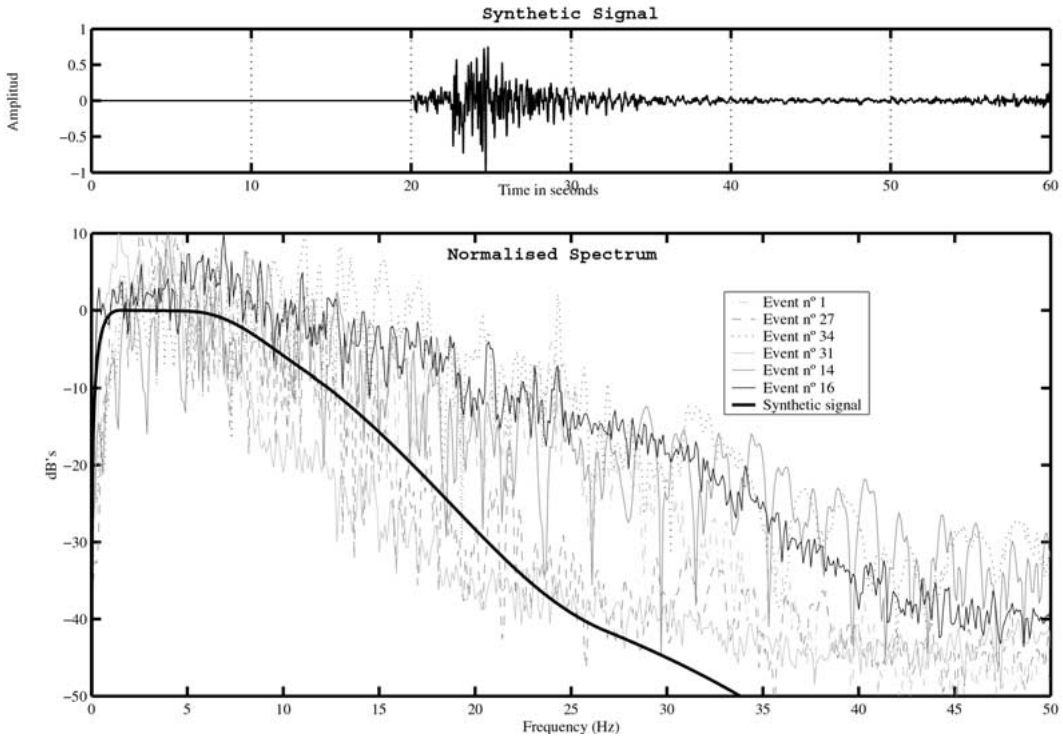

Figure 7. The Synthetic signal (**subplot 1**) and its normalised power spectrum in **subplot 2**. Also, in grey lines, six earthquake normalised spectrums (recorded by the Short Period ROA Network) are shown: **event n° 1** (99/01/08 13:09:52 'Sierra Lijar' mb = 2.5); **event n° 27** (01/04/29 17:52:30 'Alcalá de los Gazules', mb = 2.7); **event n° 34** (01/06/02 21:45:31 'Algodonales', mb = 2.3); **event n° 31** (01/05/22 03:36:33 'Argón', mb = 3.8); **event n° 14** (01/02/13 11:02:43 'Olvera', mb = 2.5) and **event n° 16** (01/02/24 11:01:21 'NE Tetuan (Morocco)', mb = 2.7). The shape of the synthetic signal is similar to the one that can be expected from real earthquakes.

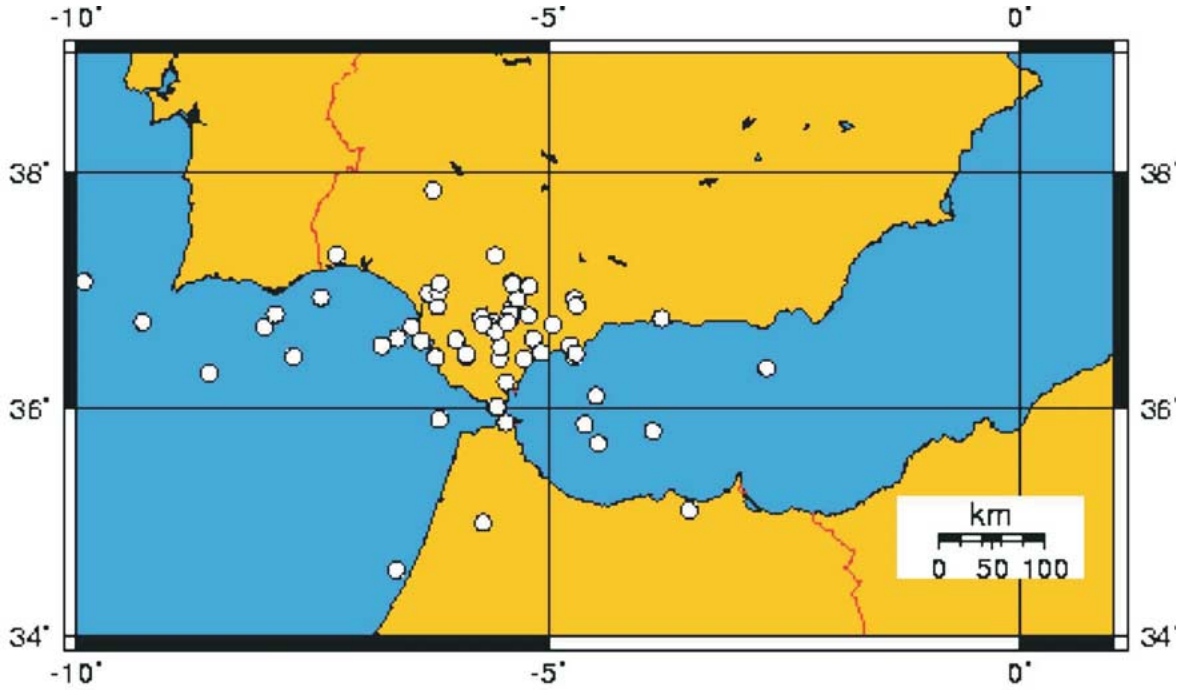

Figure 8. Earthquake database localisation.

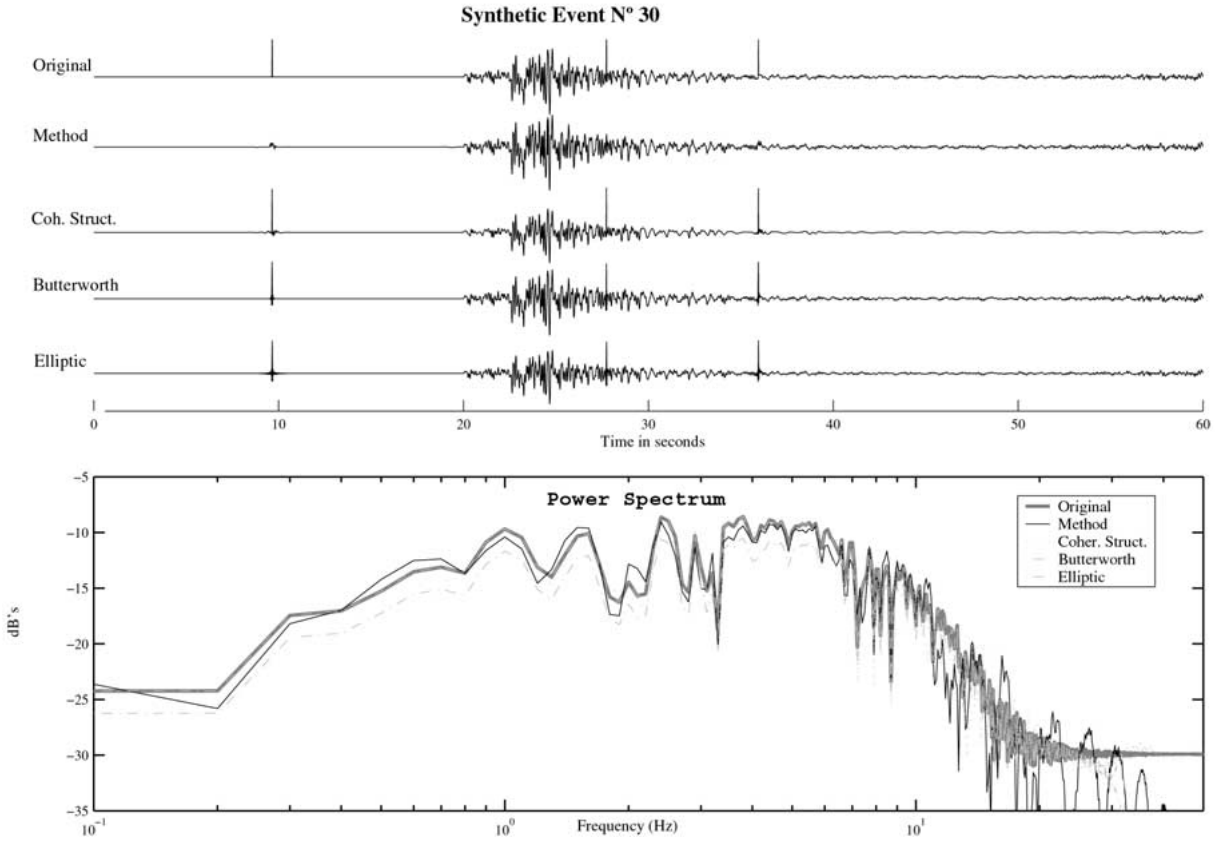

Figure 9. Synthetic signal (event n° 30) and the filtered one using the different methods: **Subplot 1. –** Original synthetic signal (event n° 30) with 3 spikes. **Subplot 2**. – Signal filtered one using the proposed method**. Subplot 3. –** Data filtered by the coherent structures method. **Subplot 4. –** Filtered by the Butterworth filter banks (a low-pass 32 Hz. was chosen). **Subplot 5. –** Filtered by the Elliptic filter banks (a low-pass 32 Hz. was selected). **Subplot 6** shows their corresponding spectrums.

- Maximum amplitude relative error. The earthquake maximum amplitude is used in the mb magnitude equations.
- Relative rms amplitude error. It is a measure of the signal similarity. This parameter will be computed using the non-noisy signal and the corresponding filtered one.
- The SNR parameter. It could be measured over the whole record, as well as on the earthquake phase arrivals. From the analyst point view, the SNR estimated on the phase picking should be considered over a short time window. Empirically, we have obtained that a two seconds window gives a good estimation of its value.

In the case of real data, it is not clear how to estimate the amplitude parameters, since the real denoised signal is unknown. Therefore, we will determine the performance of the method using a synthetic database for these parameters and, also, estimating the SNR both on the real earthquake and on the synthetic databases.

We will compare the results obtained from the proposed method with the coherent structures method and with two linear filter banks. Each linear filter bank is composed by 6 digital IIR band-pass filters (with a 0.2 Hz low cut-off frequency) and 6 low-pass filters. The high cut-off frequencies take variable values of 4, 6, 8, 10, 16 or 32 Hz chosen automatically in order to maximise the estimated P-wave SNR.

The linear filters are 4^{th} order Butterworth filter bank, and 4^{th} order Elliptic or Cauer filter bank with 1 dbs of ripple in the pass-band and a stop-band 20 dbs down.

Synthetic database

The typical seismic signal spectrum particular to this area (the Gibraltar Strait and its vicinities) shows that

Table 1. SYNTHETIC DATABASE: P-wave SNR obtained for the different methods: the proposed method, coherent structures method, Butterworth and Elliptic or Cauer filter banks. SNR was estimated using a two seconds window. Boldface numbers point out those results with higher SNR than the one given by the proposed method

	Original	Proposed method	Coherent structures	Butterworth filters	Elliptic filters
1	**–0.28**	——	**–2.37**	**–0.32**	**–21.35**
2	–0.19	13.00	–13.88	–0.12	–9.13
3	–10.38	18.10	–9.43	–8.84	–7.90
4	–20.70	–0.63	–3.80	–15.21	–7.26
5	–8.58	34.49	–8.21	–7.22	–6.42
6	**–0.05**	–8.53	**–2.40**	–13.13	**–8.13**
7	–13.91	3.92	–12.16	–6.49	0.52
8	–11.77	–2.31	–7.41	–9.11	–7.93
9	–8.18	–6.44	**–1.08**	**–5.44**	**–4.24**
10	–9.45	0.00	–1.26	–4.41	–2.93
11	–8.12	–2.93	–12.72	–3.57	**–2.23**
12	–1.67	20.90	–0.73	–1.67	–1.23
13	–4.22	20.10	–5.20	2.98	14.42
14	–0.80	14.26	–1.17	–0.84	–0.91
15	–2.82	4.93	3.40	1.19	1.93
16	0.51	34.34	2.48	0.99	1.63
17	–0.55	7.14	5.43	3.37	3.95
18	2.27	34.32	5.21	2.54	3.15
19	1.62	6.21	**9.36**	5.48	5.95
20	3.03	13.37	9.77	5.38	6.68
21	3.73	8.80	**11.98**	7.55	7.93
22	5.80	10.69	**14.29**	9.58	9.88
23	8.55	16.59	**20.54**	**16.98**	16.28
24	10.63	34.30	28.94	10.63	11.08
25	12.54	34.29	30.20	12.54	13.02
26	13.90	20.02	19.24	17.53	17.72
27	16.30	34.31	28.39	16.30	16.72
28	**21.11**	15.41	10.27	13.46	10.47
29	28.39	32.51	30.25	28.39	28.99
30	**39.31**	28.84	**29.86**	**39.32**	**39.50**

Table 2. SYNTHETIC DATABASE: entire record SNR estimation for the different methods: proposed method, coherent structures method, Butterworth and Elliptic or Cauer filter banks. Boldface numbers point out those results with higher SNR than the one given by the proposed method

	Original	Proposed method	Coherent structures	Butterworth filters	Elliptic filters
1	**–12**	——	**–2.58**	**–8.48**	**–7.79**
2	–11	5.46	–12.18	–14.71	–12.59
3	–10	23.00	–10.61	–12.78	–12.17
4	–9	5.97	–10.04	–9.42	–8.12
5	–8	47.81	–8.47	–10.19	–9.66
6	–7	3.56	2.97	–2.70	–2.50
7	–6	10.79	–6.83	–0.77	3.41
8	–5	8.19	6.00	–3.24	–4.24
9	–4	8.45	**8.82**	–2.59	2.97
10	–3	6.84	6.11	1.60	1.64
11	–2	7.95	**8.69**	2.42	2.49
12	–1	18.11	–2.88	–2.00	–0.83
13	0	20.46	–0.67	6.48	15.42
14	1	18.05	–1.46	–0.62	0.57
15	2	11.05	**12.97**	6.40	6.43
16	3	47.65	3.77	1.75	2.29
17	4	13.08	**15.05**	8.39	8.41
18	5	47.64	6.27	3.75	4.28
19	6	11.35	**17.08**	10.37	10.38
20	7	14.99	5.73	7.71	8.76
21	8	13.47	**19.10**	12.36	12.36
22	10	14.28	**21.11**	**14.34**	**14.33**
23	12	18.86	**26.21**	18.78	**18.90**
24	14	45.15	37.85	13.97	14.41
25	16	45.10	39.64	15.98	16.44
26	18	24.40	**28.44**	22.28	22.34
27	20	45.08	41.12	19.98	20.35
28	**25**	20.13	4.12	6.88	9.81
29	32	45.91	44.79	32.00	32.60
30	**64**	24.06	10.19	12.50	11.44

the energy decays very fast at high frequencies due to the waves attenuation, even for microearthquakes, whose source spectrum is nearly flat in the band of analysis. At low frequencies, the cut-off frequency (1 Hz.) is due to the instrumental response (i.e. Alguacil, 1986). Therefore, the spectrum should be smooth and almost flat between 1 to 4 or 5 Hz. We can also assume that frequencies below 0.2 Hz. are non-significant (the signal energy in this band is much smaller than the noise energy).

We have designed a synthetic record that verifies those terms. In Figure 7 we have shown the synthetic signal and its spectrum, also, in grey lines, the spectrum of six local earthquakes. The synthetic is a smooth version of the real ones.

The synthetic database is composed by 30 synthetic events with different SNR (from –12 to 64 dbs). Different types of noises have been randomly added: gaussian white noise, coloured noise, periodic noise and also real noise recorded by the ROA Short Period Network. After that, spikes were also distributed randomly along the record.

This way of creating synthetic records allows us to control exactly the SNR.

Table 3. SYNTHETIC DATABASE: Relative maximum amplitude errors (%) for the different methods: proposed method, coherent structures method, Butterworth and Elliptic filter banks. Boldface numbers point out those results with maximum amplitude errors smaller than the one given by the proposed method

	Original	Proposed method	Coherent structures	Butterworth filters	Elliptic filters
1	**100.03**	—	**49.27**	**24.77**	**33.57**
2	**43.85**	69.48	**15.10**	**22.09**	**29.94**
3	25.73	8.33	12.16	17.13	20.22
4	21.49	0.26	9.24	31.95	34.98
5	7.71	1.47	5.67	30.01	32.44
6	29.55	16.96	**12.74**	**6.95**	**7.31**
7	**1.66**	7.57	**0.19**	48.87	40.04
8	10.96	7.95	**2.57**	12.27	**3.37**
9	31.24	6.62	**5.24**	21.53	14.78
10	6.40	0.19	2.89	4.13	10.12
11	**1.22**	3.82	**1.99**	**3.19**	9.56
12	7.42	2.61	5.32	7.19	7.62
13	85.34	6.31	70.05	49.60	42.99
14	1.88	1.71	17.14	1.96	14.05
15	**0.43**	6.36	**2.03**	**0.25**	7.45
16	5.70	1.51	12.04	46.99	44.48
17	**0.16**	4.11	**2.58**	**0.78**	6.71
18	4.71	1.51	9.12	46.83	44.53
19	**0.06**	6.46	**2.51**	**1.60**	**6.12**
20	**4.68**	7.65	**4.55**	45.25	42.69
21	**0.23**	7.48	**2.84**	**2.25**	**5.65**
22	**0.37**	8.37	**3.11**	**2.77**	**5.28**
23	**0.21**	9.41	**3.76**	47.84	15.94
24	1.66	1.52	1.56	1.61	13.63
25	**1.19**	1.53	**0.12**	**1.14**	13.22
26	**0.21**	7.00	**3.86**	**3.48**	**3.56**
27	**1.10**	1.53	2.57	**1.06**	13.13
28	**0.38**	1.86	3.18	**0.33**	12.49
29	0.10	0.10	3.89	0.15	12.07
30	100.45	0.11	99.60	21.63	11.34

Table 4. SYNTHETIC DATABASE: Relative RMS amplitude errors estimated for the proposed method, coherent structures method, Butterworth and Elliptic filter banks. Results, with smaller error than the one given by the proposed method, are pointed out in boldface

	Original	Proposed method	Coherent structures	Butterworth filters	Elliptic filters
1	**113,03**	—	**7,93**	**38,01**	**31,33**
2	102,14	1,13	46,23	23,42	22,86
3	83,67	0,14	80,05	80,01	72,67
4	64,06	1,38	27,85	15,77	14,38
5	48,12	0,04	49,09	47,79	42,89
6	35,74	2,17	3,15	12,02	9,99
7	42,94	0,89	35,56	3,41	1,49
8	31,68	0,99	1,61	13,89	12,49
9	24,93	0,97	1,41	12,10	2,15
10	13,94	1,42	1,68	4,50	3,79
11	11,30	1,35	1,55	3,80	3,24
12	16,12	0,10	12,87	15,99	10,18
13	12,56	0,11	10,91	1,28	0,41
14	7,87	0,09	6,85	7,80	5,28
15	4,50	0,80	0,88	1,61	1,38
16	3,50	0,04	3,89	3,28	3,23
17	2,84	0,61	0,77	1,07	0,92
18	2,21	0,04	2,35	2,26	2,22
19	1,79	0,63	0,67	0,73	**0,62**
20	1,62	0,24	0,59	0,80	0,76
21	1,13	0,43	0,58	0,47	0,43
22	0,71	0,35	0,53	**0,31**	**0,30**
23	0,67	0,19	0,46	0,39	0,37
24	0,31	0,04	0,44	0,31	0,26
25	0,21	0,04	0,42	0,21	0,19
26	0,11	0,10	0,41	**0,08**	0,10
27	0,07	0,04	0,42	0,07	0,09
28	**0,03**	0,05	0,41	**0,03**	0,05
29	**0,01**	0,02	0,37	**0,01**	0,03
30	0,00	0,00	0,40	0,00	0,04

Real earthquake database

A real earthquake database was selected from the ROA Short Period catalogue (ROA, 2000 and 2002). This database consists of 60 records (Figure 8 shows the earthquake database localisation), chosen by taking into account their localisation, magnitude and mainly the noise content.

The Short Period ROA Network is composed by nine telemetric stations. Data is recorded, with a rate of 100 samples per second, when a STA/LTA algorithm (based on MacEvilly and Majer, 1982) is triggered. Then the record consists of a 20 seconds pre-event, the event and a post-event of 20 seconds.

The experience points out that the first 10 seconds window of the pre-event is noise, for the 98% of the records.

Discussion and results

We have applied the proposed method as well as the coherent structures method and the two linear filter bank (Butterwoth and Elliptic filters) to the synthetic and to the real earthquake databases.

Tables 1 and 2, show the SNR estimated on the P-wave and on the entire record, respectively, using the synthetic database.

The proposed method obtained the best entire record SNR in the 66.6% of the cases, and only the first event was considered noise, so the filtered output was zeroed. For the P-wave SNR, the proposed method obtained the best result in the 73.3% of the cases, and only the coherent structures method showed a significant improvement in the rest of the cases.

For the synthetic event number 30 (Figure 9), only the linear filters notably improved the original P-wave SNR, but giving a low entire record SNR due to a spike effect. The original SNR for this event in Table 2 was computed before the spikes were added.

Tables 3 and 4 show the relative amplitude errors: maximum amplitude error and the rms error respectively. The proposed method presents a maximum amplitude error smaller than 10% in 90% of the cases and a rms relative error smaller than 3 along the entire record. Only in 16.6% of the synthetic events, linear filters obtained better results for the rms error.

As before, the first synthetic event was zeroed since the method considered it as noise.

So, the proposed method obtains in 93% of the cases better results than the linear filters, and also better results than the coherent structures method in 63.4% of the cases.

Tables 5 and 6 show the P-wave and the entire record SNR estimation respectively, for the real earthquake database.

For P-wave SNR, the proposed method had the best results in the 50% of the cases, being better than the coherent structures method in the 56.6% of the cases, than the Butterworth filters in the 70% and better than Elliptic filters in the 61.6%.

Also, for the entire record SNR the proposed method obtained the best result (60%): 60% better than the coherent structures method, 85% than Butterworth filters and 81% than the Elliptic ones.

Although the coherent structure method obtained similar results as the proposed method, if it should be noticed that it deforms the waveform in the 70% of the tested events and that it does not reduce the spikes. So, this procedure is not suitable for seismic records. Figure 10 shows this effect in real event number 20 (01/03/22 at 13:06:03 'Campillo' earthquake, mb = 2.3).

The proposed method also shows the best results for spikes reduction (90%), although none of the methods eliminated them completely. Figure 11 shows the real event number 21 (01/03/28 at 12:15:17 'Jimena' earthquake, mb = 2.4), where a spike located on the P-wave arrival increased the SNR estimation.

Finally, the proposed method zeroed the real event number 56 (01/11/06 at 22:16:55 'Doñana' earthquake, mb = 2.1) due to the fact that the P-wave arrived during the first 10 seconds window of the pre-event (at 6.86 seconds), so the noise power estimation was increased.

In 97% of the tested cases (synthetic and real earthquake databases) the proposed method adapts itself better to the signal (refer to figures 9 to 11), choosing automatically the cut-off frequency.

Conclusions

We have developed a method of non-linear filtering, based on the DTWT that incorporates certain information on the type of signals we expect to register, as well as considerations on special types of noises such as spikes and periodic noise.

The proposed method adapts the coherent structure method equations to the signals and noises that are particular to the Short Period ROA Network deployed in the South of Spain. Also it incorporates two special algorithms to reduce or eliminate the periodic noises and spikes.

The results obtained, on a 30 synthetic and 60 real seismic record, show the great capacity of this method to recover the signal, even under very high noisy conditions (even down SNR of –12 dbs). The SNR (for the P-wave as well as for the entire record) was improved in the 87% of the cases. The relative rms amplitude error is less than three, and the relative maximum amplitude error less than 10% in the 90% of the synthetic events.

Acknowledgements

This work has been partially supported by the Spanish Research project of the Technology and Science Ministry Ref. REN2000-0777-C02-02, by RNM314 and by DGICYT Grant PB98-0872.

We would also thank the referees for the careful reading of this paper and for their helpful comments.

References

Alguacil, G., 1986, *Los instrumentos de una red sísmica local telemétrica para microterremotos*, La red sísmica de la Universidad de Granada, PhD-Thesis, Observatorio de la Cartuja, Facultad de Ciencias, Universidad de Granada.

Table 5. P-wave SNR for the proposed method, coherent structures method, Butterworth and Elliptic filter banks, on the real earthquake database, recorded by the Short Period ROA Network. Boldface numbers point out those results with higher SNR than the one given by the proposed method. Event number 11, marked with an '*' is an explosion

	Date		Location	mb	Est	Original	Method	Coh. St.	Butterwoth	Elliptic
1	99/01/08	13:09:52	Sierra Lijar	2.5	Lija	30.03	35.20	32.24	39.76	38.92
2	99/01/19	12:11:41	Sierra Momias	2.2	Momi	–0.16	10.61	10.48	**16.96**	**16.34**
3	99/03/11	2:57:33	Jerez	2.3	SFS	13.86	20.89	13.48	13.88	14.81
4	99/06/09	18:50:46	Mar Alboran	3.1	Lija	–19.17	–1.81	**1.61**	**2.16**	**2.61**
5	99/09/21	22:12:00	NE Grazalema	1.7	Real	23.95	24.83	**30.39**	27.83	27.84
6	99/11/18	6:55:07	Zahara Sierra	1.8	Lija	1.36	24.93	**26.11**	22.83	22.64
7	1/01/10	20:26:49	Málaga	2.5	Real	–1.41	13.04	10.30	8.98	9.86
8	1/01/15	10:47:56	Medina	2.0	Sfs	–3.91	12.09	11.28	6.61	6.34
9	1/01/15	12:58:53	Puerto Serrano	2.4	Gibl	–20.84	7.02	**15.73**	4.92	4.99
10	1/01/16	23:28:22	Casares	2.5	SCRT	–23.03	10.17	8.48	9.10	9.84
11	1/01/31	17:48:43	Torregorda*	2.5	SFS	–11.51	–4.10	**–0.41**	**–2.19**	**–1.79**
12	1/02/02	13:44:08	Alhucemas	3.7	Momi	–0.39	–0.21	–21.94	–1.57	–1.77
13	1/02/07	11:44:09	El bosque	1.5	Alj	0.86	6.33	**6.55**	5.94	6.54
14	1/02/13	11:02:43	Olvera	2.5	Lija	20.22	43.92	36.37	**45.65**	**44.32**
15	1/02/23	10:43:47	SW Coronil	2.2	Real	–8.53	11.40	8.99	9.96	10.41
16	1/02/24	11:01:21	NE Tetuan	2.7	Lija	2.29	26.28	22.12	21.91	22.66
17	1/03/09	9:25:39	Arcos	2.6	Sfs	**4.91**	4.85	**6.24**	**6.36**	**6.96**
18	1/03/13	13:19:54	Algar	2.6	momi	–0.08	5.48	–0.26	4.78	**6.85**
19	1/03/17	20:18:00	N Alborán	2.2	Real	–0.04	3.87	1.42	–5.01	–5.63
20	1/03/22	13:06:03	Campillo	2.3	Real	–3.09	18.34	**24.70**	15.33	16.03
21	1/03/28	12:15:17	Jimena	2.4	Alj	**–0.29**	–0.64	–3.75	**–0.29**	**–0.29**
22	1/04/06	6:23:15	Paterna	2.6	Scrt	–14.34	15.98	15.03	8.80	8.91
23	1/04/08	8:44:53	El bosque	2.4	Real	8.33	25.12	**26.23**	25.11	**26.48**
24	1/04/09	7:58:25	W C° S. Vicente	3.7	Scrt	–9.56	14.61	**18.75**	13.32	13.15
25	1/04/19	13:27:04	Rota	2.4	Sfs	–18.33	6.82	–0.11	1.27	2.32
26	1/04/25	2:21:13	Huelva	2.7	Scrt	–27.84	–1.40	–2.37	–3.10	–2.49
27	1/04/29	17:52:30	Alcalá Gazules	2.7	Alj	27.85	37.75	**40.70**	**41.90**	**42.38**
28	1/05/07	4:06:00	Alcacer do Sal	2.9	Lija	–0.46	17.58	10.01	15.08	15.77
29	1/05/08	19:59:15	Jubrique	1.9	Real	2.26	34.93	**38.04**	27.32	26.19
30	1/05/18	11:19:15	Grazalema	2.8	Alj	**–0.02**	–2.16	**–1.59**	**–1.13**	**–0.71**
31	1/05/22	3:36:33	Argón	3.8	Lija	29.51	29.51	**41.90**	**42.92**	**42.55**
32	1/05/24	11:57:33	Fuengirola	2.5	Real	0.63	22.72	**29.26**	19.33	19.77
33	1/05/24	13:03:17	Aracena	2.0	Alj	–0.22	17.47	1.00	3.43	3.87
34	1/06/02	21:45:31	Algodonales	2.3	Lija	28.42	45.27	44.30	**46.62**	43.42
35	1/06/08	21:35:00	Alhucemas	2.7	Lija	–6.55	5.69	9.15	11.53	12.06
36	1/06/12	19:59:31	Trafalgar	3.6	Cnil	3.97	31.64	**34.75**	**33.82**	**33.09**
37	1/06/15	12:00:16	Gribraltar	2.6	Lija	–28.70	11.54	**16.63**	10.94	11.38
38	1/06/22	1:13:55	Tetuán	3.4	Cnil	–0.03	12.36	10.75	12.08	**12.75**
39	1/06/28	15:21:47	N Marruecos	3.7	Momi	–18.28	17.02	10.08	**25.04**	**24.17**
40	1/07/11	12:10:55	E Tarifa	2.5	Alj	1.20	22.79	**32.60**	**30.06**	**29.87**
41	1/07/24	12:13:49	Algeciras	2.6	Cnil	–9.16	0.61	**4.53**	**2.00**	**1.81**
42	1/08/21	6:35:00	SE Faro	2.7	Alj	–13.70	10.86	7.70	9.36	9.86
43	1/09/01	6:00:28	S Faro	2.7	Alj	–5.55	0.87	–0.51	–0.26	0.01
44	1/09/09	3:11:34	N Marruecos	2.5	Real	–2.99	13.14	**22.09**	**14.17**	**14.50**
45	1/09/17	2:58:50	SE Faro	2.8	SCRT	–15.11	7.79	**10.94**	7.27	8.25
46	1/09/28	3:38:28	SE Bornos	2.1	Alj	–15.41	14.65	12.16	10.41	10.95
47	1/10/08	11:19:30	El Cuervo	1.7	Gibl	3.61	25.25	25.21	21.03	20.66

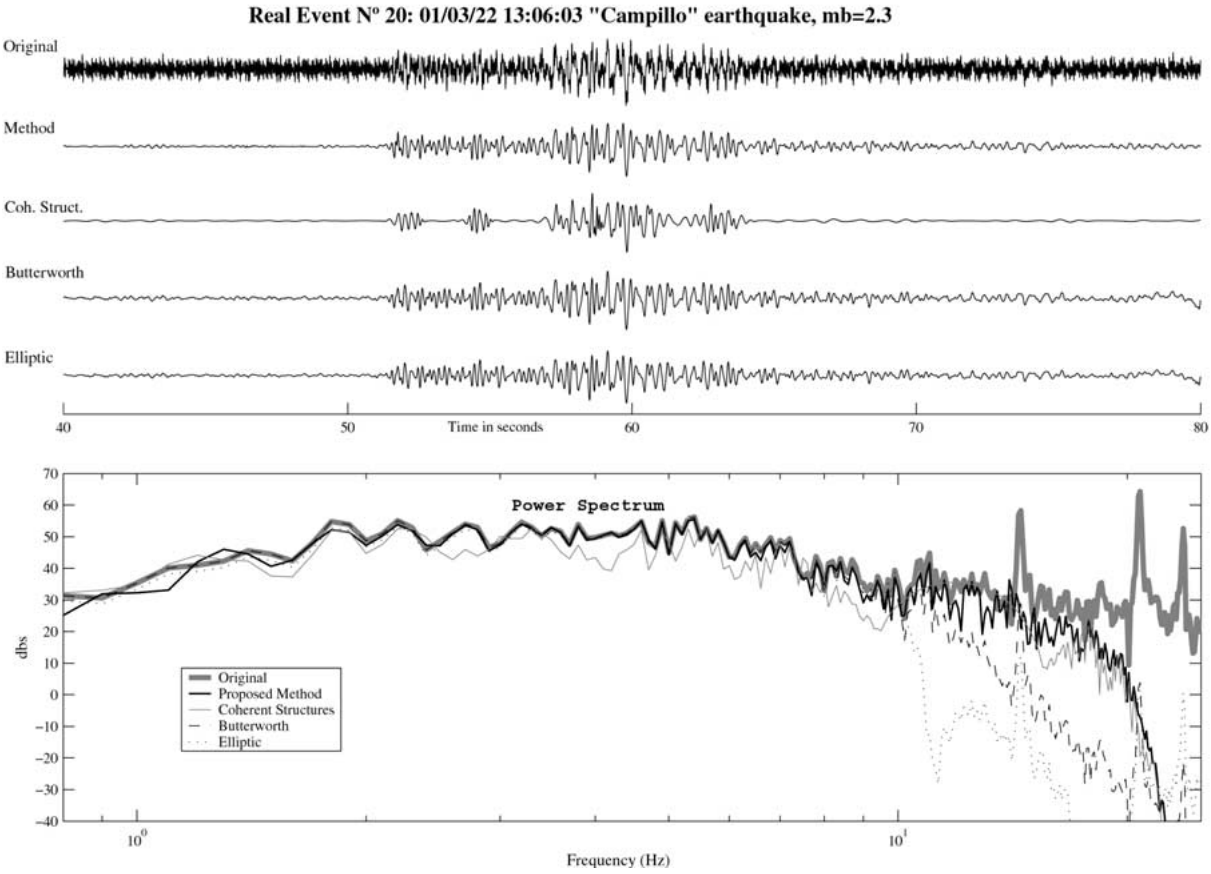

Figure 10. Real event n° 20 (01/03/22 13:06:03 'Campillo' earthquake mb = 2.3) and the filtered signals using the different methods: **Subplot 1. –** Original signal (real event n° 20). **Subplot 2. –** signal filtered by the proposed method. **Subplot 3. –** Data filtered by the coherent structures method. **Subplot 4. –** Filtered by the Butterworth filter banks (a band-pass 0.2–10 Hz filter was chosen). **Subplot 5. –** Filtered by the Elliptic filter banks (a band-pass 0.2–10 Hz. filter was selected). **Subplot 6** shows their corresponding spectrums.

Table 5. Continued

	Date		Location	mb	Est	Original	Method	Coh. St.	Butterwoth	Elliptic
48	1/10/09	9:04:10	Ronda	2.2	Real	–4.71	24.51	21.78	11.15	11.74
49	1/10/11	2:30:35	Algar	1.8	Lija	–9.79	10.29	9.24	8.69	9.40
50	1/10/15	1:11:00	Faro	2.7	Lija	–9.71	8.20	3.72	3.63	4.08
51	1/10/15	12:08:03	Estrecho Gibraltar	2.7	Alj	7.15	25.84	22.30	**32.43**	**31.59**
52	1/10/16	20:48:22	W Cádiz	2.5	Lija	2.88	25.80	22.64	18.21	18.37
53	1/10/17	14:37:06	W C° S. Vicente	3.7	Lija	–9.58	3.17	–7.44	2.08	2.68
54	1/10/27	23:56:45	Tetuán	3.6	SFS	–11.75	16.19	10.20	7.30	8.07
55	1/11/04	16:06:56	Trebujena	2.5	Gibl	–9.18	16.80	**19.01**	16.71	**17.16**
56	1/11/06	22:16:55	Doñana	2.1	Gibl	**–10.97**	—	**16.98**	**9.69**	**10.12**
57	1/11/07	8:38:10	Doñana	2.5	Gibl	–10.46	17.47	**19.17**	16.42	17.23
58	1/11/13	13:50:20	Golfo Cádiz	2.4	Cnil	–7.60	24.02	**25.94**	22.45	22.88
59	1/11/18	20:26:33	Montellano	2.3	Lija	2.65	27.25	**29.32**	24.94	25.51
60	1/11/30	10:09:24	Arcos	2.7	Cnil	–7.44	11.32	1.52	5.09	5.11

Table 6. Entire record SNR estimated by the proposed method, coherent structures method, Butterworth and Elliptic filter banks, on the real earthquake database, recorded by the Short Period ROA Network. Those results with higher SNR than the one obtained by the proposed method are pointed out in boldface. Event number 11, marked with an '*' is an explosion

	Date		Location	mb	Est	Original	Method	Coh. St.	Butterwoth	Elliptic
1	99/01/08	13:09:52	Sierra Lijar	2.5	Lija	24.71	37.06	32.75	33.73	33.37
2	99/01/19	12:11:41	Sierra Momias	2.2	Momi	–5.41	18.05	3.84	–3.32	15.70
3	99/03/11	2:57:33	Jerez	2.3	SFS	3.41	15.16	3.23	3.42	4.25
4	99/06/09	18:50:46	Mar Alboran	3.1	Lija	–15.42	17.02	**18.35**	15.80	15.10
5	99/09/21	22:12:00	NE Grazalema	1.7	Real	13.76	15.45	**23.83**	**17.52**	**17.51**
6	99/11/18	6:55:07	Zahara Sierra	1.8	Lija	–1.71	24.38	**27.22**	24.07	24.50
7	1/01/10	20:26:49	Málaga	2.5	Real	0.24	12.62	11.7	29.77	10.45
8	1/01/15	10:47:56	Medina	2.0	Sfs	–5.87	8.35	7.30	4.21	3.89
9	1/01/15	12:58:53	Puerto Serrano	2.4	Gibl	–17.55	9.24	0.84	1.71	2.91
10	1/01/16	23:28:22	Casares	2.5	SCRT	–11.56	15.07	9.91	9.92	10.13
11	1/01/31	17:48:43	Torregorda*	2.5	SFS	**15.84**	15.16	**34.08**	**28.58**	**29.54**
12	1/02/02	13:44:08	Alhucemas	3.7	Momi	–18.19	3.04	–4.97	–5.85	–5.93
13	1/02/07	11:44:09	El bosque	1.5	Alj	2.07	6.94	5.91	2.20	2.83
14	1/02/13	11:02:43	Olvera	2.5	Lija	13.92	39.34	**39.65**	**39.43**	**40.02**
15	1/02/23	10:43:47	SW Coronil	2.2	Real	–8.04	14.43	10.16	11.28	12.33
16	1/02/24	11:01:21	NE Tetuan	2.7	Lija	–3.37	19.27	16.33	15.71	16.79
17	1/03/09	9:25:39	Arcos	2.6	Sfs	4.99	9.12	7.38	6.17	6.50
18	1/03/13	13:19:54	Algar	2.6	Momi	–7.59	11.89	**12.96**	10.99	10.92
19	1/03/17	20:18:00	N Alborán	2.2	Real	**–4.53**	–15.04	**–7.33**	**–9.40**	**–9.05**
20	1/03/22	13:06:03	Campillo	2.3	Real	–4.13	20.53	**21.79**	13.61	13.71
21	1/03/28	12:15:17	Jimena	2.4	Alj	2.87	17.76	13.43	7.61	6.33
22	1/04/06	6:23:15	Paterna	2.6	Scrt	–16.14	11.18	6.15	5.49	4.78
23	1/04/08	8:44:53	El bosque	2.4	Real	8.64	26.68	**31.41**	26.10	26.71
24	1/04/09	7:58:25	W C° S. Vicente	3.7	Scrt	–15.24	9.53	**11.23**	6.69	7.00
25	1/04/19	13:27:04	Rota	2.4	Sfs	–14.31	7.76	4.89	2.53	2.45
26	1/04/25	2:21:13	Huelva	2.7	Scrt	–20.54	8.58	4.19	4.91	5.63
27	1/04/29	17:52:30	Alcalá Gazules	2.7	Alj	24.11	41.31	38.36	35.53	34.99
28	1/05/07	4:06:00	Alcacer do Sal	2.9	Lija	6.62	23.25	19.23	19.04	19.49
29	1/05/08	19:59:15	Jubrique	1.9	Real	–5.44	20.41	10.23	18.19	18.70
30	1/05/18	11:19:15	Grazalema	2.8	Alj	–11.70	10.53	**11.91**	10.45	10.22
31	1/05/22	3:36:33	Argón	3.8	Lija	30.17	33.82	**44.00**	**42.60**	**44.11**
32	1/05/24	11:57:33	Fuengirola	2.5	Real	1.52	25.45	**32.07**	21.52	21.80
33	1/05/24	13:03:17	Aracena	2.0	Alj	–16.30	13.78	5.20	4.11	5.53
34	1/06/02	21:45:31	Algodonales	2.3	Lija	18.62	38.25	**43.15**	**38.75**	**39.09**
35	1/06/08	21:35:00	Alhucemas	2.7	Lija	–1.37	21.04	17.20	17.23	16.88
36	1/06/12	19:59:31	Trafalgar	3.6	Cnil	1.24	32.10	29.98	28.81	26.93
37	1/06/15	12:00:16	Gribraltar	2.6	Lija	–15.35	20.02	18.64	17.02	17.75
38	1/06/22	1:13:55	Tetuán	3.4	Cnil	5.24	15.06	7.88	11.50	9.36
39	1/06/28	15:21:47	N Marruecos	3.7	Momi	–6.90	17.52	5.40	13.81	13.51
40	1/07/11	12:10:55	E Tarifa	2.5	Alj	0.46	21.24	**34.88**	**31.91**	**30.93**
41	1/07/24	12:13:49	Algeciras	2.6	Cnil	–11.60	11.52	8.05	6.88	7.04
42	1/08/21	6:35:00	SE Faro	2.7	Alj	–18.47	15.76	14.54	11.58	10.77
43	1/09/01	6:00:28	S Faro	2.7	Alj	2.36	11.91	**12.81**	9.64	10.23
44	1/09/09	3:11:34	N Marruecos	2.5	Real	–7.93	9.65	**13.38**	4.58	4.16
45	1/09/17	2:58:50	SE Faro	2.8	SCRT	–4.78	8.40	5.55	2.52	3.27
46	1/09/28	3:38:28	SE Bornos	2.1	Alj	–9.17	19.23	17.63	14.37	13.95
47	1/10/08	11:19:30	El Cuervo	1.7	Gibl	5.47	28.74	32.31	23.45	22.68

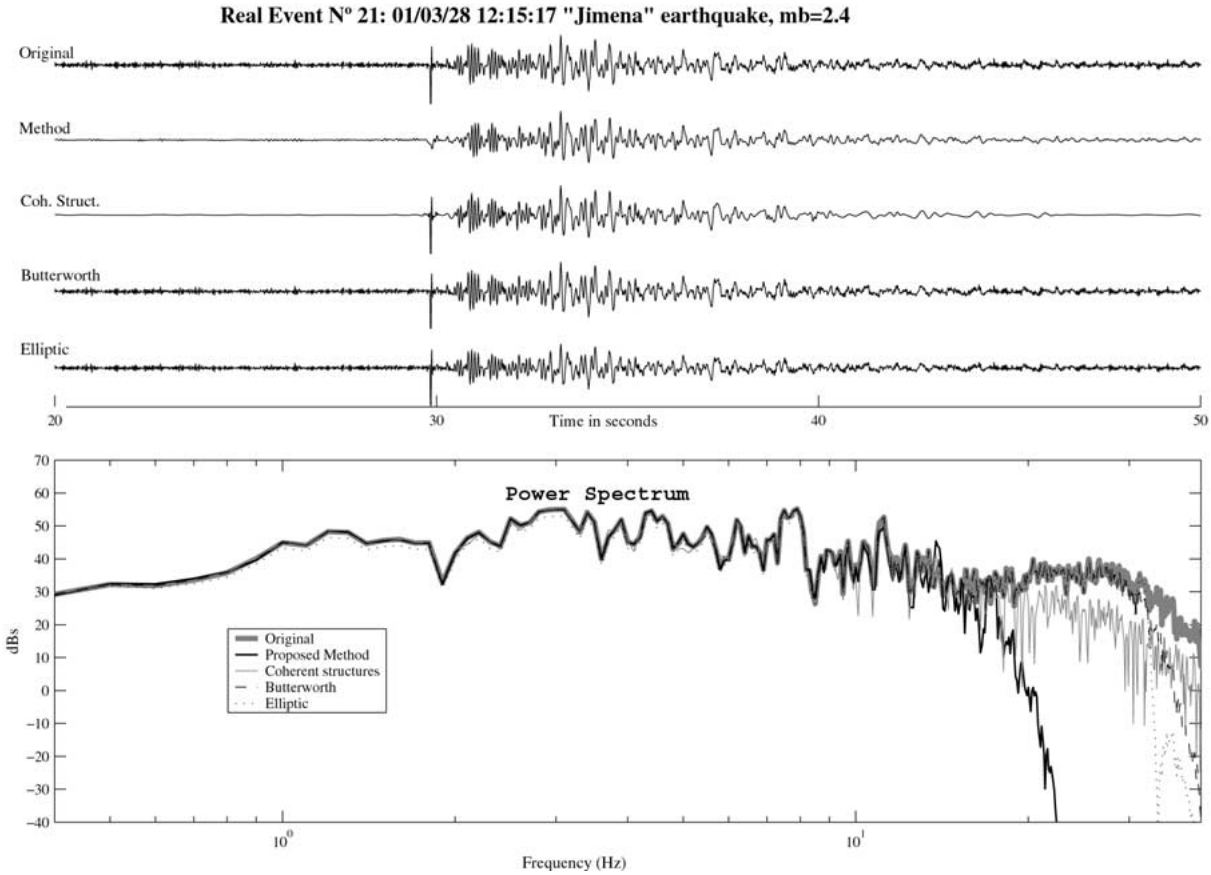

Figure 11. Real event n° 21 (01/03/28 12:15:17 'Jimena' earthquake mb = 2.4) and the filtered ones using the different methods: **Subplot 1. –** Original signal (real earthquake n° 21). **Subplot 2. –** Signal filtered by the proposed method. **Subplot 3. –** Data filtered by the coherent structures method. **Subplot 4. –** Filtered by the Butterworth filter banks (a band-pass 0.2–32 Hz filter was chosen). **Subplot 5. –** Filtered by the Elliptic filter banks (a band-pass 0.2–32 Hz. filter was selected). **Subplot 6** shows their corresponding spectrums.

Table 6. Continued

	Date		Location	mb	Est	Original	Method	Coh. St.	Butterwoth	Elliptic
48	1/10/09	9:04:10	Ronda	2.2	Real	–3.49	17.00	17.25	10.03	10.67
49	1/10/11	2:30:35	Algar	1.8	Lija	–8.44	16.34	12.10	11.19	12.25
50	1/10/15	1:11:00	Faro	2.7	Lija	–0.61	23.25	20.34	18.61	18.79
51	1/10/15	12:08:03	Estrecho Gribraltar	2.7	Alj	7.18	20.34	**33.65**	**33.56**	**33.44**
52	1/10/16	20:48:22	W Cádiz	2.5	Lija	–5.08	16.05	13.44	10.32	10.77
53	1/10/17	14:37:06	W C° S. Vicente	3.7	Lija	–5.34	17.01	**17.38**	13.97	15.47
54	1/10/27	23:56:45	Tetuán	3.6	SFS	–14.68	6.81	3.98	3.14	3.44
55	1/11/04	16:06:56	Trebujena	2.5	Gibl	–13.46	18.76	**21.73**	16.54	17.73
56	1/11/06	22:16:55	Doñana	2.1	Gibl	**–19.88**	——	**8.22**	**1.05**	**0.68**
57	1/11/07	8:38:10	Doñana	2.5	Gibl	–5.93	26.02	**31.36**	24.57	24.41
58	1/11/13	13:50:20	Golfo Cádiz	2.4	Cnil	–12.93	23.45	18.51	16.54	16.81
59	1/11/18	20:26:33	Montellano	2.3	Lija	–2.09	23.87	22.97	18.12	21.50
60	1/11/30	10:09:24	Arcos	2.7	Cnil	–4.39	9.79	2.70	2.99	2.72

Anant, Kanwaldip Singh and Dowla, Farid U., 1997, Wavelet transform methods for phase identification in three-component seismograms, *Bull. Seism. Soc. Am.* **87**(6), 1598–1612.

Andrew J. Michael, Stephen P. Gildea and Jay J. Pulli, 1982, A real-time digital seismic event detection and recording system for network applications, *BSSA* **72**(6), 2339–2348.

Donoho, D.L., 1994, *De-noising by Soft-thresholding*, Manuscript, Dept. of Statistics, Stanford Univ. Available at `http://www.stat.stanford.edu/~donoho/Reports/index.html`

Evans, J.R. and Allen, S.S., 1983, A teleseismic-specific detection algorithm for a single short-period traces, *BSSA* 73(4), 1173–1186.

Fedorenko, Y.V. and Husebye, E.S., 1999, First breaks – automatic phase pickings of P- and S-onsets in seismic records, *Geophys. Res. Lett.* **26**(21), 3249–3252.

Freeden, W. and Schneider, F., 1998, An integrated wavelet concept of physical geodesy, *J. Geodesy* **72**, 259–281.

Gledhill, K.R., 1985, An earthquake detector employing frequency domain techniques, *BSSA* **75**(6), 1827–1835.

Goforth, T. and Herrin, E., 1981, An automatic seismic signal detection algorithm based on the Walsh Transform, *BSSA* **71**(4), 1351–1360.

Lilly, J.M. and Park, J., 1995, Multiwavelet spectral and polarization analyses of seismic records, *Geophys. J. Int.* **122**, 1001–1021.

Mallat, S., 1998, *A Wavelet Tour of Signal Processing*, Academic Press, San Diego, USA.

McEvilly, T.V. and Majer, E.L., 1982, ASP: An automated seismic processor for micro-earthquake networks, *BSSA* **72**(1), 303–325.

Moltshan, G.M., Pissarenko, V.F. and Smirnova, N.A., 1964, Some statistical methods of detecting signals in noise, *Geophys. J.* **8**(3), 319–323.

Ridsdill-Smith, T.A. and Dentith, M.C., 1999, The wavelet transform in aeromagnetic processing, *Geophysics* **64**(4), 1003–1013.

ROA, 2000, *Anales 1999. Observaciones Meteorológicas, Sísmicas y Geomagnéticas*, Real Instituto y Observatorio de la Armada en San Fernando, San Fernando, Spain.

ROA, 2002, *Anales 2001. Observaciones Meteorológicas, Sísmicas y Geomagnéticas*, Real Instituto y Observatorio de la Armada en San Fernando, San Fernando, Spain.

Ulrych, T.J., Sacchi, M.D. and Graul, J.M., 1999, Signal and noise separation: Art and science, *Geophysics* **64**(5), 1648–1656.